Influence of surface modification on the *in vitro* corrosion rate of magnesium alloy AZ31

Joy E. Gray-Munro, Christine Seguin, Michael Strong
Department of Chemistry and Biochemistry, Laurentian University, Sudbury, Ontario, Canada P3E 2C6

Received 25 September 2007; revised 20 May 2008; accepted 9 June 2008
Published online 23 September 2008 in Wiley InterScience (www.interscience.wiley.com). DOI: 10.1002/jbm.a.32205

Abstract: In recent years, magnesium alloys have been proposed as a new class of metallic bioabsorbable implant material. Unfortunately, the production of hydrogen gas and an increase in alkalinity are both by-products of the degradation process of these materials. This necessitates the development of magnesium alloys with controlled degradation rates. Furthermore, biocompatible coatings that can delay the onset of corrosion would ensure that the mechanical integrity of the implant remains intact in the early stages of healing. This article explores the influence of surface modification by biomimetic calcium phosphate coating, biodegradable polymer coatings, and acid etching on the corrosion rate of the AZ31 magnesium alloy in simulated body fluid. Our results indicate that all of these surface treatments have a positive impact on the corrosion rate of the material and that in the early stages of implantation it is possible to tailor the corrosion rate through an appropriate choice of surface treatment. © 2008 Wiley Periodicals, Inc. J Biomed Mater Res 91A: 221–230, 2009

Key words: calcium phosphate coating; magnesium; corrosion; polymer coating; surface modification

INTRODUCTION

Inert metals such as titanium and its alloys, stainless steel, and cobalt–chromium alloys are commonly used for load-bearing orthopedic implants. Although these metals have proven to be effective in providing the required mechanical support during the healing process, stress shielding can occur resulting in decreased implant stability long term. Furthermore, corrosion and wear of these materials can result in the release of toxic particles, with subsequent inflammation and tissue loss. In many cases, such as fracture fixation, these implants are only necessary for a short time until healing and union of tissue has occurred, but to remove them, a second, costly, surgery would be required. To overcome the need for this second surgery, biodegradable implants have been proposed. These materials would provide the necessary stability in the initial stages of healing and would gradually be replaced by bone as they degraded.

Correspondence to: J. E. Gray-Munro; e-mail: jgray@laurentian.ca

Contract grant sponsors: Natural Sciences and Engineering Research Council, Canada Foundation for Innovation

Magnesium alloys have recently been proposed as a new class of biodegradable implant material.[1] These materials have a number of advantages over traditional metallic biomaterials such as their high strength to weight ratio, inherent biocompatibility,[2–6] and mechanical properties that are similar to bone.[1] Preliminary *in vivo* animal studies have demonstrated that a magnesium alloy implanted in the femura of guinea pigs was completely replaced by new bone formation within 18 weeks[6] and that magnesium based alloys may be a promising material for cardiovascular applications.[3,7,8] Bone remodeling around open-porous magnesium alloy scaffolds has also been observed.[5]

Magnesium-based metals readily corrode in aqueous solutions at pH values below 11; this means that under physiological conditions these materials will readily degrade according to the following reactions:

$$Mg^0 \rightarrow Mg^{2+} + 2e^-$$

$$2H_2O + 2e^- \rightarrow H_2 \uparrow + 2OH^-$$

The typical corrosion product is magnesium hydroxide. This film acts to passivate the surface in pure water, but in the presence of other common anions such as chloride, the passive film is disrupted, soluble magnesium compounds are formed,

and corrosion continues. Hydrogen gas evolution and an increase in alkalinity are both by-products of the corrosion reaction and pose significant health risks for the patient.

The corrosion of these materials in simulated body fluid (SBF) has not been extensively studied. It has been demonstrated that the polarization of pure magnesium in SBF is similar to that observed in NaCl; however, AC impedance studies indicated that the mechanism is likely not the same.[9]

Pure magnesium has been shown to corrode at a rate that is much too high for biomedical applications[9]; however, alloying has been shown to slow the corrosion rates of magnesium-based metals.[9] It has also been observed that the *in vitro* corrosion rate of these materials is faster than the *in vivo* corrosion rate.[10] Furthermore, one study found that the AZ91 alloy demonstrated improved corrosion resistance *in vitro* but poor *in vivo* behavior while the opposite was observed for the LAE442 alloy.[10] This result indicates that the *in vitro* and *in vivo* corrosion mechanisms are not necessarily the same.

The fast corrosion of magnesium necessitates the development of magnesium alloys with controlled degradation rates to minimize the production of toxic by-products. Furthermore, biocompatible coatings that can delay the onset of corrosion would ensure that the mechanical integrity of the implant remains intact in the early stages of healing.

It has been demonstrated that heat treatment of the materials has an impact on the microstructure of the alloy and impacts their corrosion resistance.[11] Surface treatment by alkali heat treatment,[11] anodizing,[9] and titanium ion implantation[12] have been shown to have a positive impact on the corrosion rate of magnesium alloy materials in simulated biological fluid. However, surface treatment with hydrofluoric acid was shown to have no impact on the corrosion rate of pure magnesium in SBF.[13]

An ideal coating for biodegradable magnesium alloys must be corrosion resistant in the early stages of healing, nontoxic, and biocompatible. The ability to promote bioactivity/osteointegration is also essential. Both calcium phosphate and biodegradable polymer coatings are promising candidates for this purpose.

Calcium phosphate as calcium-deficient carbonate hydroxyapatite is the main mineral component of bone.[14] Calcium phosphate coatings have been shown to improve the biocompatibility of metallic implants and to increase bone growth at the site of implantation.[15,16] In particular, biomimetically deposited coatings have received recent attention because of their excellent biocompatibility and ability to promote osseointegration.[17–20]

Poly(lactic acid) (PLA) is a semicrystalline biodegradable polymer.[21] The stereoisomer L-PLA is preferred for biomedical applications because hydrolysis results in the production of L(+)-lactic acid, which is found naturally in the body. Furthermore, the degradation products are nonacidic. PLA is of particular interest for orthopedic applications because it has been demonstrated that bone-like apatite can be deposited on PLA fibers.[22] The structure of this polymer is shown in Figure 1.

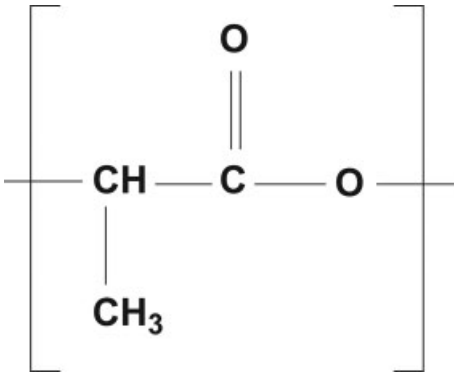

Figure 1. Chemical structure of poly(L-lactic acid) (PLA).

Poly(desaminotyrosyl tyrosine hexyl carbonate) [poly(DTH carbonate)] is one of the relatively new classes of tyrosine-derived polycarbonate polymers. These polymers are based on the natural amino acid tyrosine and they have desirable mechanical properties for use in orthopedic devices. These are amorphous polymers that biodegrade to produce an alcohol and desaminotyrosyl tyrosine as their degradation products. It is expected that *in vivo*, the desaminotyrosyl tyrosine will enzymatically degrade to desamino tyrosine and L-tyrosine, both found naturally in the body.[23] Furthermore, direct bone apposition on the surface of poly(DTH carbonate) implants has been observed[24,25] and is believed to be a result of ionic interaction of calcium ions with the carboxylate groups formed during the degradation of the polymer.[24] The structure of the poly(DTH carbonate) polymer used in this study is shown in Figure 2. In this study, the influence of acid etching in phosphoric acid, calcium phosphate coatings, PLA coatings, and poly(DTH carbonate) coatings on the *in vitro* corrosion rate of magnesium alloy AZ31 in SBF has been examined. Acid etching in phosphoric acid was chosen because it is a convenient method for surface cleaning, it should improve the adhesion of any subsequent coating, and the magnesium phosphate layer that is formed at the surface contains elements already found in bodily fluid meaning it is nontoxic. The calcium phosphate and polymer coatings were all chosen because of their known ability to promote calcium phosphate deposition *in vivo*. This is an essential requirement for implants with the ability to promote osseointegration. AZ31

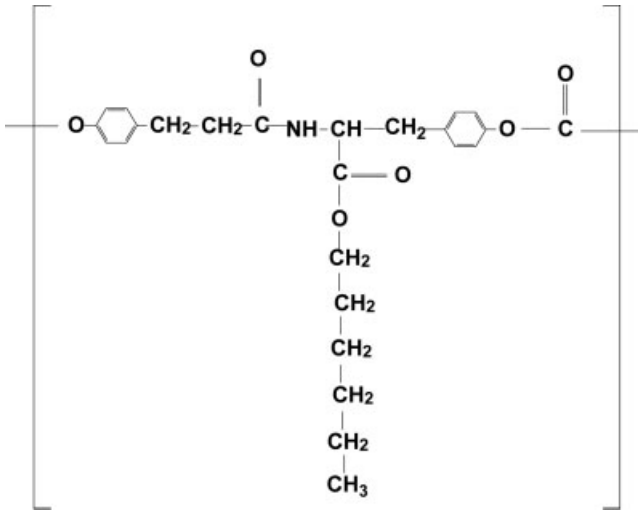

Figure 2. Chemical structure of poly(desaminotyrosyl tyrosine hexyl carbonate) [poly(DTH carbonate)].

was chosen for this study for three reasons: (1) it contains a relatively small amount of potentially toxic aluminum, (2) its mechanical properties have been shown to be a good match to bone,[4] and (3) it has been shown to degrade *in vivo* at a similar rate as AZ91 and WE43.[10] This makes it the optimum choice because AZ91 contains more aluminum and WE43 contains several rare earth elements that are known to have moderate toxicity.

EXPERIMENTAL DETAILS

Materials

The AZ31 MgAlZn 1-mm-thick foil was obtained from Alfa Aesar and was cut into 1 × 2 cm^2 samples. The trichloroethylene, sodium carbonate, sodium hydroxide, $CaCl_2 \cdot H_2O$, Na_2HPO_4, HCl, HNO_3, PLA, and poly(DTH carbonate) used for coating the samples were all obtained from Sigma-Aldrich. Both the 4-(2-hydroxyethyl)piperazine-1-ethanesulfonic acid (HEPES) buffer and SBF were also purchased from Sigma-Aldrich. The composition of the SBF is given in Table I.

Surface modification

Acid etching

The magnesium alloy coupons were degreased by sonication in acetone for 15 min, followed by sonication in distilled water for 15 min prior to etching. The samples were etched in a 90% (v/v) phosphoric acid solution at 55°C for 30 s. The etched samples were subsequently neutralized in 100 g/L NaOH solution for 30 s. The neutralized samples were then rinsed with distilled water for 30 s and air dried.

Calcium phosphate coating

Prior to calcium phosphate coating the magnesium alloy coupons were etched according to the procedure described earlier. The calcium phosphate coating bath consisted of a solution of 3 m*M* $CaCl_2 \cdot 2H_2O$ and 1.8 Na_2HPO_4, respectively. These concentrations were chosen to ensure that a Ca/P ratio of 1.67:1, the stoichiometric ratio of Ca/P in hydroxyapatite, was maintained. The initial pH of the coating bath was adjusted to a pH of 5 using either hydrochloric acid or sodium hydroxide as required. The acid-etched magnesium coupons were immersed in the Ca/P bath for a period of 2 weeks at ambient temperature and then air dried.

Polymer coating

The polymer coatings were spray-coated onto both sides of the acid-etched magnesium alloy coupons from a 5% (w/v) solution of either PLA or poly(DTH carbonate) in methylene chloride. The samples were then allowed to air dry.

In vitro evaluation of corrosion rate

SBF was prepared by dissolving ~7 g of HEPES in 1 L of Hank's balanced salt solution. Three samples were prepared for each type of surface modification. Static immersion tests are most commonly used for the evaluation of orthopedic implant materials. In keeping with this trend, each sample was immersed in 50 mL of SBF adjusted to pH 7 at 37°C ± 0.5°C with one key difference. Every 24 h, for a 2-week period, the magnesium alloy coupons were immersed in a new SBF bath to ensure the pH remained near physiological values (6.3–7.8). This was necessary because the corrosion of the magnesium alloy results in both a significant increase in solution pH and an increase in magnesium ion concentration in the bath. Both of these factors result in a decrease in the *in vitro* corrosion rate; however, *in vivo* the electrolyte would be dynamic in nature and equilibrium concentrations of magnesium ions as well as high pH conditions would not be maintained.[10] After 24 h the SBF solutions were diluted using 2% HNO_3. The concentration of magnesium and calcium in the solutions was quantified by flame atomic absorption. All aqueous magnesium determinations were done using a Perkin-Elmer

TABLE I
Composition of Simulated Body Fluid

Component	Concentration (g/L)
$CaCl_2 \cdot 2H_2O$	0.185
$MgSO_4$ (anhydrous)	0.09767
KCl	0.4
KH_2PO_4	0.06
$NaHCO_3$	0.335
NaCl	8.0
Na_2HPO_4 (anhydrous)	0.04788
D-Glucose	1.0

5000 flame atomic spectrophotometer. For magnesium determinations, a wavelength of 285.5 nm was used with a current of 5 mA. Optimal flame conditions were achieved using a C_2H_2/air ratio of 30/40 and the scan time was 0.5 s. The concentration of magnesium in the SBF solution prior to corrosion was also measured and subtracted from the overall change in concentration of these ions due to the corrosion process. The experiment was repeated in triplicate for each type of surface modification. The reported values are an average of the three experiments.

Surface characterization

The surfaces of the coated magnesium alloy coupons were characterized by a combination of ATR-FTIR and scanning electron microscopy (SEM)/EDS before and after corrosion in SBF for 2 weeks. This combination of techniques allowed us to characterize changes in both the surface chemistry and morphology that occur upon immersion of the coated magnesium alloy coupons in SBF. A separate paper[26] details the composition of the calcium phosphate coatings as characterized by X-ray photoelectron spectroscopy and X-ray diffraction.

SEM/EDS

Samples to be analyzed were sputter coated with a thin film of carbon to render the sample conductive. All samples were analyzed in the Zeiss EVO50 SEM, EDS spectrometer. The vacuum in the chamber was 1.14×10^{-6} mbar. The beam current of the electron gun was set at 1.0 nA. A spot size of 520 nm was used with a working distance of 8.5–9 mm. The collection time for the EDS was set for 45 s.

ATR-FTIR analysis

ATR-FTIR spectra were collected using a Bruker Optics infrared microscope with an ATR objective with a ZnSe crystal. The resolution of the spectrometer was 4 cm^{-1}. Each spectrum is the result of 1000 scans. The spectrometer was equipped with a MCT detector that was liquid nitrogen cooled. The spectra were corrected for CO_2 and H_2O with the atmospheric compensation function of the software.

RESULTS AND DISCUSSION

In this study, the influence of acid etching, calcium phosphate coating, and polymer coating with PLA and poly(DTH carbonate) on the *in vitro* corrosion rate of magnesium alloy AZ31 in SBF has been examined. The alloy used for these studies was a rolled foil purchased from Alfa Aesar. It should be noted that the corrosion resistance of magnesium alloys depends on the chemical composition as well as the microstructure of the material.[27] The microstructure of the material can be strongly affected by mechanical processing and in fact the corrosion resistance of magnesium alloy AZ31 in SBF has been shown to be influenced by processing conditions.[28] The *in vitro* corrosion rates have been monitored by incubating magnesium alloy coupons in SBF at 37°C and monitoring the amount of magnesium dissolved as a function of time. The surface chemistry and morphology of the coatings before and after corrosion has been examined by a combination of SEM/EDS and ATR-FTIR analysis. In particular, the ability of these coatings to promote calcium phosphate deposition has been determined by the detection of calcium phosphate species at the surface using these techniques.

Influence of acid etching

Acid etching is a common pretreatment in preparation for surface coating. Acid etching of magnesium alloys is believed to remove the gross scale that is produced during the manufacturing process and to replace the native oxide layer with a more passive oxide layer.[29] Figure 3 shows SEM images of a magnesium alloy coupon that has been solvent degreased [Fig. 3(a)] and a sample that has been etched in phosphoric acid [Fig. 3(c)]. It is clear from these images that prior to acid etching the sample surface has a nonuniform morphology with visible pits, whereas the acid-etched sample is much more homogeneous. To obtain coatings with minimum porosity and maximum adhesion a uniform surface is desirable.

Acid etching also results in significant changes in the surface chemistry of the magnesium alloy coupons. Figure 4 shows ATR-FTIR spectra for a magnesium alloy coupon before and after acid etching. Two new vibrational bands are observed in the infrared spectrum after etching. The new vibrational band at 3700 wavenumbers is the OH stretching vibration for magnesium hydroxide.[30] This compound readily forms at the surface of magnesium alloys due to exposure with air or aqueous solutions, particularly at higher pH values.[31] Following the acid etching step the samples are neutralized in a solution of sodium hydroxide. It is likely that the magnesium hydroxide forms at this stage. The new vibrational band centered at 1030 cm^{-1} is due to the presence of phosphate on the etched surface and is most likely present as magnesium phosphate. Figure 5(c) shows the phosphate region of this spectrum in more detail. One broad band is observed between 900 and 200 cm^{-1}. This band represents the symmetric (v1) and antisymmetric (v3) stretching modes of phosphate.[32] The fact that this band is broad and featureless is indicative of PO_4^{3-} in an amorphous

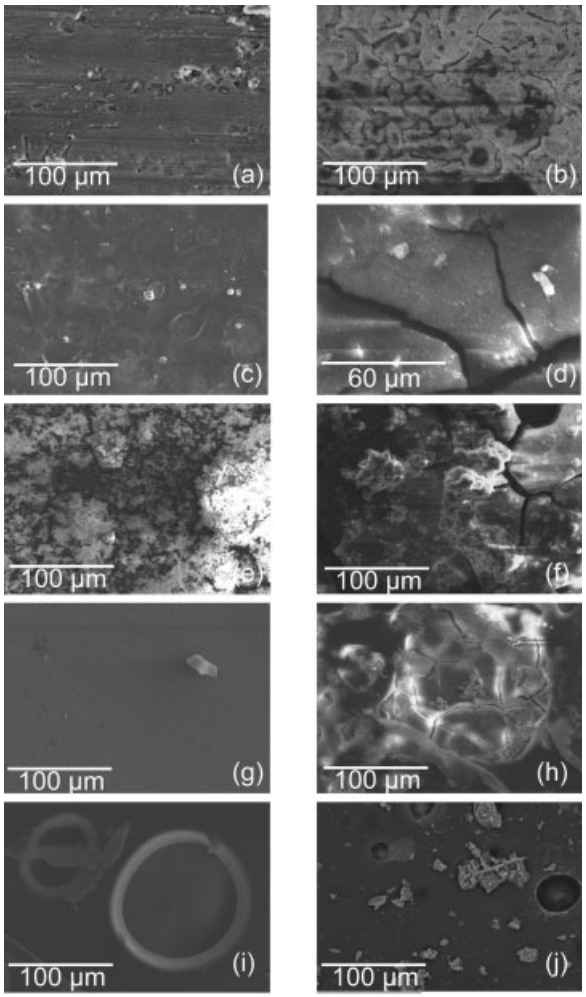

Figure 3. Scanning electron micrographs of magnesium alloy before and after corrosion in SBF at 37°C for 2 weeks; (a) solvent-degreased sample prior to corrosion, (b) solvent-degreased sample after corrosion, (c) acid-etched sample prior to corrosion, (d) acid-etched sample after corrosion, (e) calcium phosphate-coated sample prior to corrosion, (f) calcium phosphate-coated sample after corrosion, (g) PLA-coated sample prior to corrosion, (h) PLA-coated sample after corrosion, (i) poly(DTH carbonate)-coated sample prior to corrosion, and (j) poly(DTH carbonate)-coated sample after corrosion.

compound.[32] In fact, the formation of magnesium phosphate films during etching in phosphoric acid has been previously observed.[33] The following reactions have been proposed for magnesium alloys with acidic phosphate solutions[33]:

$$Mg \rightarrow Mg^{2+} + 2e^- \quad (1)$$

$$2H^+ + 2e^- \rightarrow H_2 \uparrow \quad (2)$$

$$3Mg^{2+} + 2H_2PO_4^- \rightarrow Mg_3(PO_4)_2 + 3H_2 \uparrow \quad (3)$$

In the first reaction, anodic dissolution of magnesium occurs because of its instability at pH values less than 11, and this is coupled with the reduction of hydrogen (reaction 2). Indeed, hydrogen bubbles were observed during etching of our samples. Finally, magnesium phosphate precipitates onto the surface of the alloy because of its low solubility. The presence of phosphorus was detected on our acid-etched samples by XPS analysis at 0.3 atomic %. A high (21.8%) atomic percentage of sodium was also observed in the XPS spectrum. The source of this sodium is likely in the form of a thin layer of sodium hydroxide that is adsorbed to the sample during the neutralization step.

Figure 6 is a graph of the total mass of magnesium dissolved into the SBF solution as a function of immersion time in the bath. A steep rise in the concentration of dissolved magnesium in the bath is observed in the first 150 h (6 days) for the nonacid-etched (clean) samples. This steep rise represents a corrosion rate of 31 mg/day in the initial stages of corrosion, whereas in the latter stages the corrosion rate slows to 14 mg/day. The observed decrease in the corrosion rate indicates that the alloy becomes somewhat passivated, likely because of the deposition of a surface film on the alloy. The corrosion rate for the acid-etched sample (9 mg/day) is substantially lower than that of the nonacid-etched samples. Furthermore, the corrosion rate is constant for the duration of the study. It is obvious from this graph that acid etching results in a dramatic improvement in corrosion resistance of the magnesium alloy in SBF.

It is evident that the improved uniformity of the surface coupled with the magnesium hydroxide/magnesium phosphate layer that is produced by acid etching helps to protect the alloy from corrosion in SBF.

Figure 3(b,d) shows SEM images of the clean and acid-etched magnesium alloys after corrosion in SBF, and Figure 5(b,d) shows the corresponding FTIR

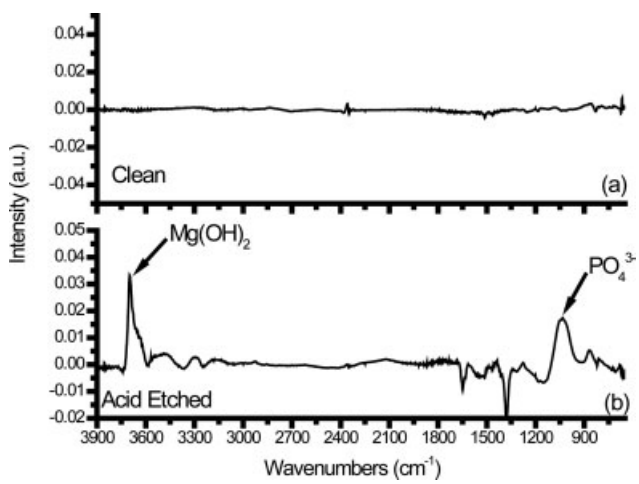

Figure 4. ATR-FTIR spectra of (a) solvent degreased (clean) and (b) acid-etched magnesium alloy coupons prior to corrosion.

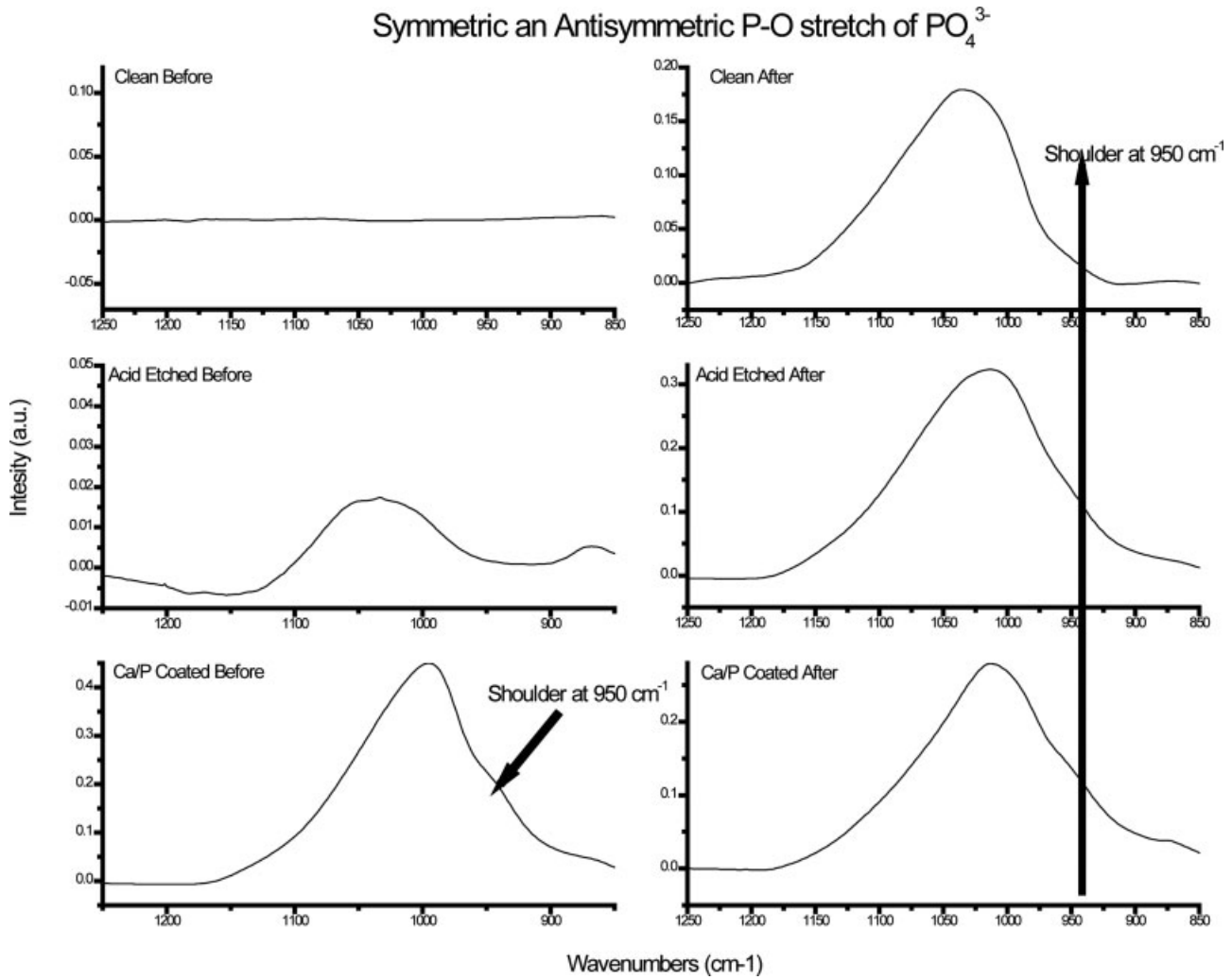

Figure 5. ATR-FTIR spectra of the phosphate region for cleaned, acid-etched, and calcium phosphate-coated samples before and after corrosion in SBF at 37°C for 2 weeks; (a) solvent-degreased sample prior to corrosion, (b) solvent-degreased sample after corrosion, (c) acid-etched sample prior to corrosion, (d) acid-etched sample after corrosion, (e) calcium phosphate-coated sample prior to corrosion, and (f) calcium phosphate-coated sample after corrosion.

spectra. The main feature in both the FTIR spectra is a large broad peak from 900 to 1200 cm^{-1} due to the P—O stretching vibrational modes. Calcium and phosphate ions are both present in the SBF solution. As the sample corrodes, the pH of the solution rises inducing precipitation of calcium phosphate onto the sample surface.

It has been shown that amorphous calcium phosphate has one large broad featureless band in this region. As the crystallinity of the calcium phosphate improves (i.e., as hydroxyapatite is formed), the observed peak becomes narrower and a high frequency shoulder emerges between 950 and 970 cm^{-1}.[32,34] The IR spectrum for the clean sample after immersion in SBF shows one broad band with a very weak shoulder at about 950 cm^{-1}. This is consistent with the presence of very poorly crystalline HA at the surface. The poor crystallinity is to be expected due to the high corrosion rate of the

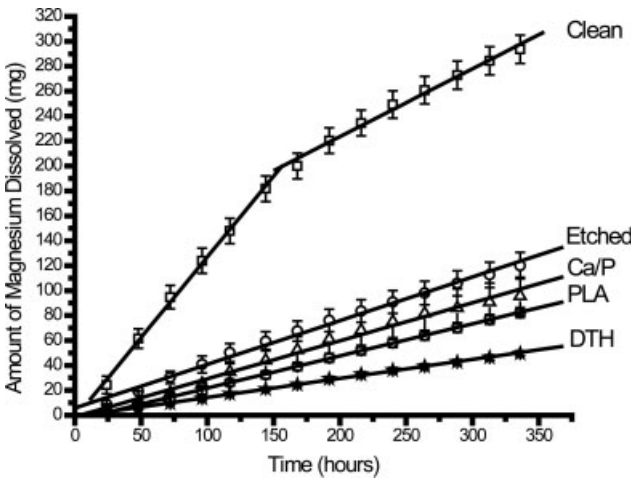

Figure 6. Amount of magnesium dissolved as a function of immersion time in SBF at 37°C for solvent-degreased (clean), acid-etched, calcium phosphate-coated, PLA-coated, and poly(DTH carbonate)-coated magnesium alloy coupons.

unmodified material and the fact that magnesium ions are a known crystal growth inhibitor for HA.[37] In contrast, the crystallinity of the calcium phosphate deposited on the corroded acid-etched sample is improved as evidenced by the increase in intensity of the v_1 P—O stretch vibrational band at 950 cm^{-1}. Chemical analysis by EDS confirms the presence of both calcium and phosphorus on the surface of the corroded samples, confirming that calcium phosphate is deposited on the surface of the magnesium alloy during corrosion. Furthermore, the SEM images [Fig. 3(b,d)] indicate that the calcium phosphate layer that forms on the acid-etched sample is more uniform. The improved crystallinity and more uniform morphology of the calcium phosphate layer on the acid-etched sample can both be correlated to the slower corrosion rate of the acid-etched sample, a result of the magnesium phosphate/magnesium hydroxide layer that helps to protect the surface from corrosion. This means there is more time for heterogeneous nucleation and subsequent growth of the calcium phosphate crystals. Therefore, although both samples are partially passivated by the formation of a calcium phosphate film, the layer that forms on the acid-etched sample is more protective, resulting in a lower overall corrosion rate.

Because of the decrease in corrosion rate observed for acid-etched samples, all subsequent samples have been pretreated by acid etching prior to coating application.

Influence of calcium phosphate coating

Acid-etched samples were immersed in a calcium phosphate coating bath for 2 weeks in order to precoat the magnesium alloy coupons with calcium phosphate. Figure 5(e) shows an ATR-FTIR spectrum for the calcium phosphate coating. The main feature in this FTIR spectrum is a large broad peak between 900 and 1200 cm^{-1} with a distinct shoulder at 950 cm^{-1}. As previously discussed this is indicative of the presence of poorly crystalline hydroxyapatite ($Ca_{10}(PO_4)_6(OH)_2$).[32,34] Our previous studies on the deposition of calcium phosphate coatings on magnesium alloys have shown that the mechanism of apatite deposition on the magnesium alloy substrate can be summarized by the following three reactions[26]:

Step 1: $Mg \rightarrow Mg^{2+} + 2e^-$ and $2H_2O + 2e^- \rightarrow H_2\uparrow + 2OH^-$

Step 2: $H_2PO_4^- \rightarrow HPO_4^{2-} \rightarrow PO_4^{3-}$

Step 3: $(10 - x)Ca^{2+} + xMg^{2+} + 6PO_4^{3-} + 2OH^- \rightarrow (Ca_{(1-x)}Mg_x)_{10}(PO_4)_6(OH)_2$

We have observed that the deposition process is catalyzed by the anodic dissolution of the magnesium substrate. A detailed analysis of the composition of the coating by XPS, XRD, SEM/EDS, and FTIR has been previously published.[26] These results indicate that the final coating is primarily a magnesium-rich/calcium-deficient hydroxyapatite.[26]

Figure 3(e) is an SEM image of the calcium phosphate coating prior to corrosion in SBF. It is clear from this image that the coating is present as two distinct layers. The underlayer very closely resembles the calcium phosphate layer that we observed on the acid-etched samples after corrosion [Fig. 3(d)]. The formation of this layer is catalyzed by the anodic dissolution of the substrate as described earlier. The overlayer is calcium phosphate precipitates that form in solution via a homogeneous nucleation process as the pH of the coating bath rises over time.

Figure 6 shows a graph of the total mass of magnesium dissolved into the SBF solution as a function of immersion time in the bath for calcium phosphate-coated samples. The overall *in vitro* corrosion for the calcium phosphate-coated samples is constant with a corrosion rate of ~7 mg/day. This is only slightly less than the 9 mg/day corrosion rate that was observed for samples that have not been precoated with calcium phosphate. An SEM image of the calcium phosphate-coated magnesium coupon after corrosion in SBF for 2 weeks is shown in Figure 3(f). Prior to corrosion the coating had a double layer structure. After corrosion only one layer is observed. The fact that the previously observed overlayer of calcium phosphate precipitates disappears suggests that dissolution of the overlayer occurs in the early stages of immersion in the SBF bath. The dissolution of the coating is followed by film growth as evidenced by the increase in Ca/Mg ratio measured by EDS. These results show that the Ca/Mg ratio increases from 1.01 prior to corrosion to 18.2 after corrosion; this indicates that the thickness of the calcium phosphate layer has increased significantly. The ATR-FTIR spectrum [Fig. 5(f)] again shows a large broad peak between 900 and 1200 cm^{-1} with a distinct shoulder at 950 cm^{-1}, indicating that the calcium phosphate film is poorly crystalline hydroxyapatite ($Ca_{10}(PO_4)_6(OH)_2$.[32,34]

Overall, these results indicate that the calcium phosphate coating did not have a significant effect on the overall corrosion rate of the material. However, the calcium phosphate coating did induce further nucleation and growth of calcium phosphate at the surface of the alloy which may be beneficial for improved osseointegration.

Influence of polymer coating

Acid-etched samples were spray-coated with either PLA or poly(DTH carbonate). These polymers were chosen because they are biodegradable poly-

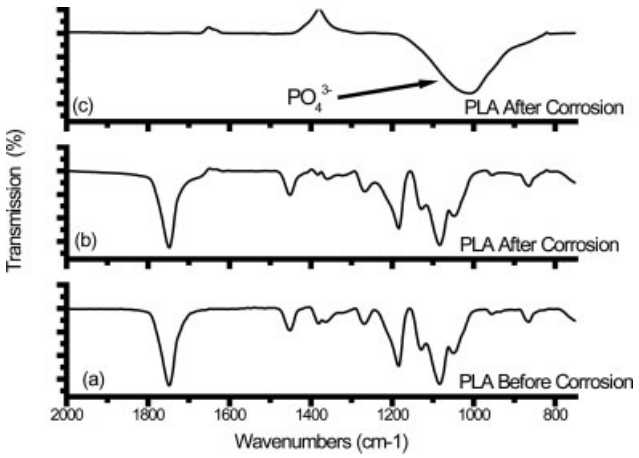

Figure 7. ATR-FTIR spectra of PLA-coated magnesium alloy coupons before and after corrosion in SBF at 37°C for 2 weeks; (a) prior to corrosion, (b) region 1 after corrosion, and (c) region 2 after corrosion.

mers, have nontoxic degradation products, and have been shown to induce calcium phosphate deposition *in vivo*.[24] Figure 6 is a graph of the total mass of magnesium dissolved into the SBF solution as a function of immersion time in the bath for the polymer-coated samples. The overall *in vitro* corrosion for both the polymer-coated samples is constant with a corrosion rate of ~5.6 mg/day for PLA and 3.5 mg/day for poly(DTH carbonate). In comparison with uncoated acid-etched samples the PLA and poly (DTH carbonate) coatings decrease the corrosion rate of the magnesium alloy by a factor of 2 and 3, respectively.

The ATR-FTIR spectra for the PLA-coated magnesium coupons before and after corrosion are shown in Figure 7. Infrared spectra were obtained for three different corroded samples in multiple areas on each sample. Two very different infrared spectra were obtained depending on the area of the corroded sample that was analyzed. In Figure 7(b), there is no difference in the IR spectra for PLA after corrosion compared with the polymer prior to corrosion. This indicates that the polymer coating has not degraded in this region. In Figure 7(c), all of the polymer peaks have disappeared. One large broad peak between 900 and 1200 cm^{-1} with a distinct shoulder at 950 cm^{-1} is observed which is again consistent with that of the phosphate band in poorly crystalline hydroxyapatite. Chemical analysis by EDS confirms the presence of both calcium and phosphorus on the corroded sample. The infrared data suggest that the degradation of the coating is nonuniform. SEM images of the PLA-coated samples before and after corrosion [Fig. 3(g,h)] show that the PLA coating prior to corrosion is a uniform layer, whereas after corrosion it is obvious that pores have formed in the coating. The morphology of the corroded regions within these pores and the ATR-FTIR spectra are both similar to our previously observed spectra for corroded acid-etched magnesium alloy coupons. Furthermore, the EDS spectra obtained revealed that the pores contained high atomic percents of calcium and phosphorous.

The ATR-FTIR spectra for poly(DTH carbonate)-coated magnesium coupons before and after corrosion are shown in Figure 8. Infrared spectra were obtained for three different corroded samples in multiple areas on each sample. Two different infrared spectra were observed depending on the area of the corroded sample that was analyzed. In Figure 8(b), there is no difference in the IR spectra for poly(DTH carbonate) after corrosion compared with the polymer prior to corrosion. This indicates that the polymer coating has not degraded significantly in this region. In Figure 8(c), the infrared spectrum is almost identical to that of the noncorroded sample. However, there is one important change, a new large broad between 900 and 1200 cm^{-1} with a distinct shoulder at 950 cm^{-1} large broad is observed, which is consistent with the phosphate band in poorly crystalline hydroxyapatite. Chemical analysis by EDS confirms the presence of both calcium and phosphorus on the surface of these samples. The fact that the phosphate band is superimposed on the characteristic infrared spectrum of the polymer implies that the calcium phosphate has precipitated on top of the polymer coating.

SEM images of the poly(DTH carbonate)-coated samples before and after corrosion [Fig. 3(i,j)] show that the poly(DTH carbonate) coating prior to corrosion is relatively uniform with some circular structures. EDS analysis confirmed that these circular regions were actually polymer "droplets" and not

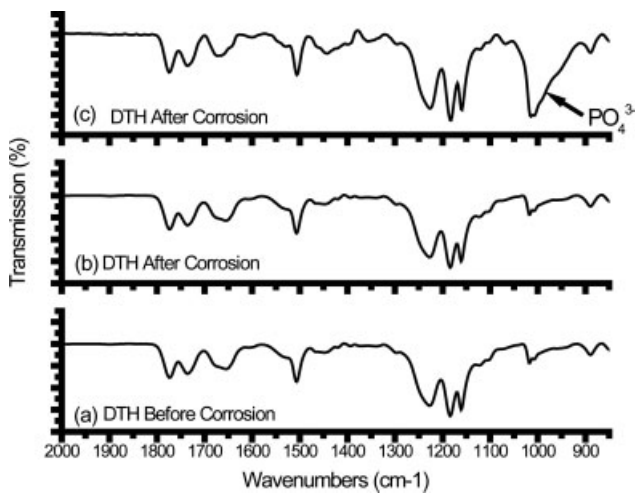

Figure 8. ATR-FTIR spectra of poly(DTH carbonate)-coated magnesium alloy coupons before and after corrosion in SBF at 37°C for 2 weeks; (a) prior to corrosion, (b) region 1 after corrosion, and (c) region 2 after corrosion.

pores in the coating itself. After corrosion the SEM image clearly shows that the polymer film is largely intact with some precipitates deposited on top of the polymer surface.

Comparison of polymer coatings

Comparing the corrosion behavior of the two polymer coatings yields two very important differences. The first is that the corrosion rate of the poly (DTH carbonate) coating is about half that of the PLA coating. In both cases it is likely that the corrosion initiates at defect sites in the coating, in particular at the edges of the samples where the polymer film may be less uniform. Chemical analysis of the polymer samples by EDS prior to corrosion shows that a significant amount of magnesium (12.76 atomic %) is present at the surface of PLA-coated samples, whereas no magnesium is observed on poly (DTH carbonate)-coated samples. After corrosion, the calcium, phosphorus, and magnesium are detected on both samples, but in the case of PLA-coated samples the detected concentration of magnesium has decreased to 3.5 atomic % while an increase to 6 atomic % magnesium is observed on the poly(DTH carbonate)-coated samples. The observed decrease in magnesium concentration coupled with the observation that calcium phosphate deposition occurs only in areas where the polymer has completely degraded for the PLA-coated samples suggests that the degradation of the polymer and corrosion of the substrate initiates at small pores (not visible by SEM) in the polymer coating. The anodic dissolution of the underlying magnesium results in deposition of calcium phosphate in these regions. The original defect sites thus become coated with calcium phosphate, resulting in the observed decrease in magnesium concentration at the surface of the corroded samples.

The second important observation is that for the poly(DTH carbonate)-coated samples the calcium phosphate is deposited on top of the polymer coating. It is likely for these coatings that corrosion initiates at the edges of the sample where the coating is less uniform. The resulting increase in solution pH induces homogeneous nucleation and growth of calcium phosphate in solution, followed by precipitation onto the polymer surface. Overall, it is clear that the uniformity of the polymer coating has a significant impact on the overall corrosion rate of the magnesium alloy substrates.

CONCLUSIONS

Figure 9 compares the corrosion rates of all of the surface modification strategies employed in this study. The comparison reveals that the corrosion rates of the surface-treated magnesium alloys decreased in the following order:

Clean > Acid Etched > Calcium Phosphate Coated > PLA Coated > Poly(DTH carbonate) Coated.

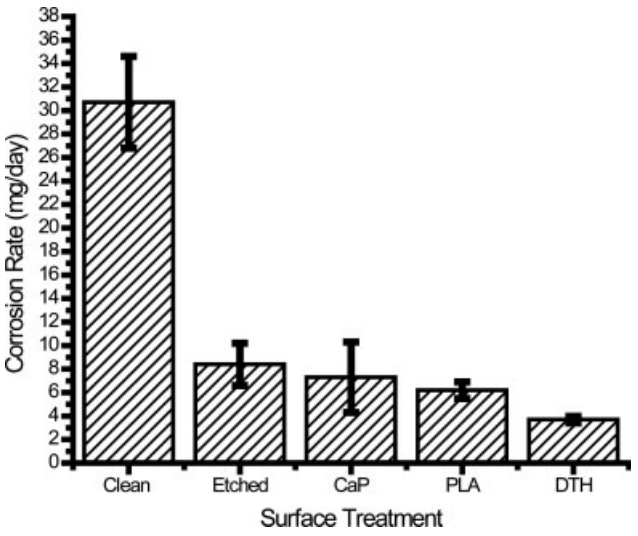

Figure 9. Summary of corrosion rates for all surface-modified magnesium alloy samples.

Although the overall corrosion rates of the surface-modified materials vary, all of these coatings induced the deposition of calcium phosphate onto the surface of the implant. This is an important feature for improved bioactivity/osseointegration of metal implant materials. This study has demonstrated that surface modification can be used to control the corrosion rate of magnesium based implant materials to minimize the production of toxic by-products. Furthermore, the corrosion rates can be tailored for specific applications by appropriate coating selection.

References

1. Staiger MP, Pietak AM, Huadmai J, Dias G. Magnesium and its alloys as orthopedic biomaterials: A review. Biomaterials 2006;27:1728–1734.
2. Li LC, Gao JC, Wang Y. Evaluation of cyto-toxicity and corrosion behavior of alkali-heat-treated magnesium in simulated body fluid. Surf Coat Technol 2004;185:92–98.
3. Waksman R, Pakala P, Kuchulakanti PK, Baffour R, Hellinga D, Seabron R, Tio FO, Wittchow E, Hartwig S, Harder C, Rohde R, Heublein B, Andreae A, Waldmann KH, Haverich A. Safety and efficacy of bioabsorbable magnesium alloy stents in porcine coronary arteries. Catheter Cardiovasc Interv 2006;68:607–617.
4. Witte F, Ulrich H, Rudert M, Willbold E. Biodegradable magnesium scaffolds. I. Appropriate inflammatory response. J Biomed Mater Res A 2007;81:748–756.
5. Witte F, Ulrich H, Palm C, Willbold E. Biodegradable magnesium scaffolds. II. Peri-implant bone remodeling. J Biomed Mater Res A 2007;81:757–765.

6. Witte F, Kaese V, Haferkamp H, Switzer E, Meyer-Lindenberg A, Wirth CJ, Windhagen H. *In vivo* corrosion of four magnesium alloys and the associated bone response. Biomaterials 2005;26:3557–3563.
7. Levesque J, Dube D, Fiset M, Mantovani D. Investigation of corrosion behaviour of magnesium alloy AM60B-F under pseudo-physiological conditions. Mater Sci Forum 2003;426:521–526.
8. Waksman R, Pakala R, Hellinga D. Effect of bioabsorbable magnesium alloy stent on neointimal formation in a porcine coronary. Eur Heart J 2006;26:1222–1226.
9. Song GL. Control of biodegradation of biocompatible magnesium alloys. Corros Sci 2007;49:1696–1701.
10. Witte F, Fischer J, Nellesen J, Crostack HA, Kaese V, Pisch A, Beckmann F, Windhagen H. *In vitro* and *in vivo* corrosion measurements of magnesium alloys. Biomaterials 2006;27: 1013–1018.
11. Liu CL, Xin YC, Tang GY, Chu PK. Influence of heat treatment on degradation behavior of bio-degradable die-cast AZ63 magnesium alloy in simulated body fluid. Mater Sci Eng A 2007;456:350–357.
12. Liu CG, Xin YC, Tian XB, Zhao J, Chu PK. Corrosion resistance of titanium ion implanted AZ91 magnesium alloy. J Vac Sci Technol A 2007;25:334–339.
13. Lopez HY, Cortes DA, Escobedo S, Mantovani D. In vitro bioactivity assessment of metallic magnesium. Key Engi Mater 2006;309–311:453–456.
14. Hench LL, Best S. Ceramics, glasses and glass-ceramics. In: Ratner B, Hoffman A, Schoen FJ, Lemons JE, editors. Biomaterials Science—An Introduction to Material in Medicine. London: Elsevier Academic Press; 2004. p 165–167.
15. Dorozhkin SV, Epple M. Biological and medical significance of calcium phosphates. Angew Chem Int Ed Engl 2002;41: 3130–3146.
16. Puleo DA, Nanci A. Understanding and controlling the bone-implant interface. Biomaterials 1999;20:2311–2321
17. Chakraborty J, Sinha M, Basu K. Biomolecular template-induced biomimetic coating of hydroxyapatite on and SS 316 L substrate. J Am Ceram Soc 2007;90:1258–1261.
18. Zhang E, Yang K. Biomimetic coating of calcium phosphate on biometallic materials. Trans Nonferrous Met Soc China 2005;15:1199–1205.
19. Li F, Feng Q, Cui F, Li H, Schubert H. A simple biomimetic method for calcium phosphate coating. Surf Coat Technol 2002;154:88–93.
20. Zhang QY, Leng Y. Electrochemical activation of titanium for biomimetic coating of calcium phosphate. Biomaterials 2005;26:3853–3859.
21. Kohn J, Abramson S, Langer R. Bioresorbable and bioerodable materials. In: Ratner B, Hoffman A, Schoen FJ, Lemons JE, editors. Biomaterials Science—An Introduction to Material in Medicine. London: Elsevier Academic Press; 2004. p 115.
22. Yuan X, Mak AFT, Li J. Formation of bone-like apatite on poly(L-lactic acid) fibers by a biomimetic process. J Biomed Mater Res 2001;57:140–150.
23. Bourke SL, Kohn J. Polymers derived from the amino acid L-tyrosine: Polycarbonates, polyarylates and copolymers with poly(ethylene glycol). Adv Drug Deliv Rev 2003;55:447–466.
24. Choueka J, Charvet JL, Koval KJ, Alexander H, James KS, Hooper KA, Kohn J. Canine bone response to tyrosine-derived polycarbonates and poly (L-lactic acid). J Biomed Mater Res 1996;31:35–41.
25. James K, Levene H, Parsons JR, Kohn J. Small changes in polymer chemistry have a large effect on the bone-implant interface: Evaluation of a series of degradable tyrosine-derived polycarbonates in bone defects. Biomaterials 1999;20: 2203–2212.
26. Gray JE, Strong M. The mechanism of deposition of calcium phosphate coatings from solution onto magnesium alloy AZ31. J Biomed Mater Res A 2009;90A:339–350.
27. Pardo A, Merino MC, Coy AE, Arrabal R, Viejo F, Maytkina E. Corrosion behaviour of magnesium/aluminum alloys in 3.5 wt% NaCl. Corros Sci 2008;50:823–834.
28. Wang H, Estrin Y, Fu H, Song G, Zuberova Z. The effect of pre-processing and grain structure on the bio-corrosion and fatigue resistance of magnesium alloy AZ31. Adv Eng Mater 2007;9:967–972.
29. Gray JE, Luan B. Protective coatings on magnesium and its alloys: A critical review. J Alloys Compd 2002;336:88–113.
30. Yu S, Hariram KP, Kumar R, Cheang P, Aik KK. *In vitro* apatite formation and its growth kinetics on hydroxyapatite/polyetherketone biocomposites. Biomaterials 2005;26:2343–2352.
31. Fotea C, Callaway J, Alexander MR. Characterisation of the surface chemistry of magnesium exposed to the ambient atmosphere. Surf Interface Anal 2006;38:1363–1371.
32. Pleshko N, Boskey A, Mendelsohn R. Novel infrared spectroscopic method for the determination of crystallinity of hydroxyapatite minerals. Biophys J 1991;60:786–793.
33. Zhao M, Wu S, An P, Luo J. Influence of surface pretreatment of the chromium-free conversion coating of magnesium alloy. Mater Chem Phys 2007;103:475–483.
34. Antonakos A, Liarokapis E, Leventouri T. Micro-raman and FTIR studies of synthetic and natural apatites. Biomaterials 2007;28:3043–3054.